ISSN 1062-7391, Journal of Mining Science, 2016, Vol. 52, No. 4, pp. 778–792. © Pleiades Publishing, Ltd., 2016.
Original Russian Text © V.A. Chanturia, E.L. Chanturia, I.Zh. Bunin, M.V. Ryazantseva, E.V. Koporulina, A.L. Samusev, N.E. Anashkina, 2016, published in Fiziko-Tekhnicheskie Problemy Razrabotki Poleznykh Iskopaemykh, 2016, No. 4, pp. 142–157.

MINERAL DRESSING

Effect of Acid and Electrochemical Treatment on Physicochemical and Electrical Properties of Tantalite, Columbite, Zircon and Feldspar

V. A. Chanturia*, E. L. Chanturia, I. Zh. Bunin, M. V. Ryazantseva, E. V. Koporulina, A. L. Samusev, and N. E. Anashkina

Institute of Integrated Mineral Development—IPKON, Russian Academy of Sciences, Kryukovskii tupik 4, Moscow, 111020 Russia
**e-mail: vchan@mail.ru*

Received June 3, 2016

Abstract—The article gives a report on integrated experimental research into targeted change of chemical and phase composition of surface and increase in contrast of physicochemical, electrical and electrochemical properties of tantalite, columbite and zircon under treatment by acid product of water electrolysis—anolyte (pH < 5) and by muriatic solution (HCl, pH 3–3.5). The X-ray photoelectron spectroscopy, high resolution spectroscopy and chemical and electrophysical techniques reveal the mechanism of structural–chemical surface transformation of tantalite, columbite, zircon and feldspar under leaching in acid solutions; this surface transformation mechanism consists in activation of dissolving of iron- and silicate-containing surface films and high-rate oxidation of iron atoms in surface layer of tantalite and columbite, with transition of Fe(II) to Fe(III) and surface destruction of zircon, with formation of oxygen-vacant defects of SiO_3^{2-} and SiO_2^0 type under influence of anolyte.

Keywords: Tantalite, columbite, zircon, feldspar, quartz, X-ray photoelectron spectroscopy, microscopy, physicochemical and electric properties, anolyte and HCl solution treatment of minerals.

DOI: 10.1134/S1062739116041190

In the Russian Federation main niobium and tantalum reserves occur in poor unconventional–type ores in endogenous (primary) deposits [1, 2], The ores of potentially commercial grade are specified with low rare metals content (Nb_2O_5 content ranges within hundredth of tenths of a percent in Nb–Ta ores) and a variety of accompanying impurities: phosphorus, iron, titanium, rare earths, strontium, barium, torium, (metasomatites with tantalum-bearing pyrochlore and columbite [2]) or beryllium, rubidium, cesium, and stannum (granites and pegmatites).

The actual and up to now unsolved niobium–tantalum ore processing problem deals with the difficulty to produce conditioned concentrates adequate for further chemical and metallurgical treatment because of structural and textural specific features of niobium–tantalum ores, fine dissemination and intensive rare-metal minerals intergrowth. Moreover, the efficient flotation recovery of the concentrates is often hampered or even impossible owning to the presence of iron oxides and hydroxides films on surface of the minerals to be separated. Iron oxides and hydroxides films smooth the physicochemical properties of mineral surface concerned. In flotation with complexing collecting agents (hydroxamic acids) iron valency on mineral surface plays the constitutive role, as the stability constant (lg K) of trivalent iron hydroxamate is appreciably higher as compared to that of bivalent iron hydroxamate, they are 11.4 and 4.8, respectively [3].

The present research aims at investigation into the mechanism for purposeful modification of surface composition and enhancement of discrepancy in physicochemical, electrochemical, electrical, and mechanical properties of rare metal minerals: tantalite, columbite, zircon and rock–forming minerals: quartz, feldspar. With this target in view the researchers processed the study minerals and mineral

suspensions with acid product of electrochemical treatment of water, namely, with anolyte at pH < 5, this product exhibiting high oxidizing activity in leaching and oxidation of mineral surface [4]. HCl solution of pH 3–3.5 which was usually applied in well-known processes for preparation of Ta–Nb gravity concentrates to flotation, was used in reference tests [1, 2].

1. STUDY MATERIALS AND PROCEDURES

The study objects were rare metal minerals (of perfect formula: tantalite $(Fe, Mn)(Ta, Nb)_2O_6$; columbite $(Fe, Mn)(Nb, Ta)_2O_6$, where content of basic elements in columbite without minor impurities, mass %: Nb—71.8, Ta—2.68, Fe_{total}—10.48, Fe(II)—8.07, Fe(III)—2.05, Mn—9.22; zircon $ZrSiO_4$, mass %: Zr+Hf—63.88, Si—9.66, Fe_{total}—1.08, Fe(II)—0.62, Fe(III)—0.46), produced from rough gravity concentrates in the gravity–magnetic–electrical flowsheet. Host rock minerals, mass %: Si—91.32, Fe_{total}—0.35, Fe(II)—0.22, Fe(III)—0.13 and feldspar, mass %: Si—70.57, Al—10.58, K—11.09, Na—1.16, Ca—0.67, Fe_{total}—0.92, Fe(II)—0.52, Fe(III)—0.40. The gross elementary composition of specimens was evaluated by atomic–emission spectroscopy with inductively coupled plasma (Varian Vista CCD Simultaneous ICP–AES).

The data on chemical composition of minerals obtained by the analytical scanning electron microscopy are summarized in Table 1. ***Tantalite*** contained negligible amount of impurities Ti^{4+} and Sn^{4+} (Table. 1), as a whole its composition complied with niobic manganesian–tantalite $(Mn_{0.80}Fe^{2+}_{0.15}Fe^{3+}_{0.05})_{1.00}(Ta_{1.15}Nb_{0.80}Ti_{0.03}Sn_{0.02})_{2.00}O_{6.00}$.

Grains of columbite $(Mn_{0.91}Fe^{2+}_{0.08}Fe^{3+}_{0.01})_{1.00}(Nb_{1.79}Ta_{0.20}Ti_{0.01})_{2.00}O_{6.00}$ were monomineral fraction of $-3+0.5$ mm. The bulk of zircon of -300 μm in size contained isomorphic impurity Hf^{4+} and hydroxyl groups; the composition of specimens was described by formula $(Zr_{0.85}Hf_{0.03})_{0.88}[Si_{1.00}O_{3.52}(OH)_{0.48}]$.

The crystalline mineral structure of columbite group is referred to structural brookite type with distorted closest packing of oxygen atoms along axis *a* [5] (Fig. 1). Nb, Ta, and Fe, Mn cations occupy ½ of octahedral voids, arranging ridged columns along axis *c*. Thereto, the fiber-wise sequence of two (Nb, Ta) and one (Fe-, Mn) columns occur along axis *a* [5]. Semiconductive minerals: columbite and tantalite refer to complex oxide class of the general formula $A_mB_nX_p$ (AB_2X_6), with *n*-type conductivity and low surface conductance: $4.0\cdot10^{-7}$ $Ohm^{-1}\cdot cm^{-1}$ for columbite, $6.5\cdot10^{-7}$ $Ohm^{-1}\cdot cm^{-1}$ for tantalite [6]. Thermoelectric coefficient α_{tec} (μV/deg) is 150 [6, 7], 125 [8] for columbite, 20 [7, 8] for tantalite.

Table 1. Chemical composition of tantalite, columbite, zircon, and feldspar specimens, mass%

Compound	Tantalite	Columbite	Zircon	Feldspar	
				chesterlite	chesterlite
Nb_2O_5	24.3	68.8	—	—	—
Ta_2O_5	58.2	12.6	—	—	—
SiO_2	—	—	35.1	67.2	65.9
TiO_2	0.6	0.3	—	—	—
SnO_2	0.5	0.0	—	—	—
ZrO_2	—	—	60.9	—	—
HfO_2	—	—	4.0	—	—
Al_2O_3	—	—	—	18.0	17.3
MnO	13.0	16.8	—	—	—
FeO	3.4	1.5	—	2.0	0.3
Na_2O	—	—	—	2.5	—
K_2O	—	—	—	10.3	16.5
Nb/Ta	0.4	5.4	—	—	—
Zr/Hf	—	—	15.0	—	

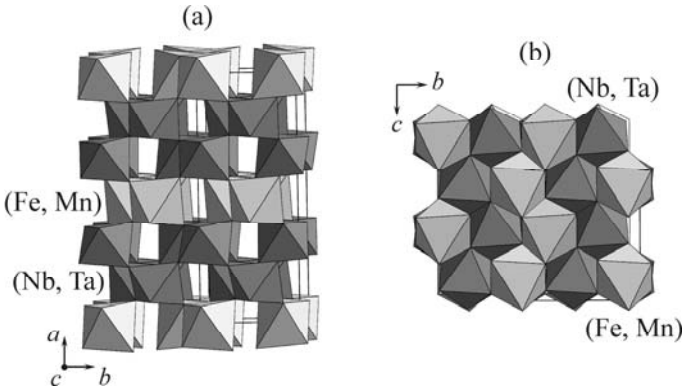

Fig. 1. Crystalline structure of columbite–tantalite mineral group (Fe, Mn)(Nb, Ta)$_2$O$_6$ in (a) axonometric and (b) *bc* projections.

Finely dispersed mineral specimens were treated with anolyte (pH 3.5–3.7, Eh 800–950 mV, dissolved oxygen concentration being ~ 24 mg/l) and HCl solution (pH 3.5) for 1 hour, next the liquid phase was decanted, the content of Fe, Mn, and Si ions was assessed by chemical and atomic adsorption. The anolyte was produced in diaphragm electrolyzer with an anode covered with oxide–ruthenium at current concentration I_v = 0.4–0.6 A/l and 25 min electrochemical treatment of water.

The specimen composition and morphology were studied on polished sections and discrete mineral grains by analytical scanning electron microscopy (SEM–low–vacuum scanning electron microscope Jeol JSM 5610LV equipped with INCA Oxford 450 energy-dispersed analyzer and LEO 1420VP−INCA Oxford 350 microscope) and scanning probe microscopy (modular scanning probe microscope Ntegra Prima, NT–MDT, Zelenograd). Sections and mineral grains were fixed by two-sided graphite scotch; the thin conductive graphite layer was plated on specimen surface, if required.

Specific micromorphology features of mineral surface were examined in details by atomic force microscopy at semi-contact mode in air at room temperature with the use of mid-hard probes (cantilevers) (NSG10) with gold reflective covering, at resonance frequency ~ 240 kHz and rigidity constant ~ 11.8 N/m; radius of needle curvature being 10 nm. In some cases supplementary information was obtained when concurrently with AFM-patterns of sample surface topography its phase contrast images were fixed under variations in cantilever oscillation phase ($\Delta\Theta$) whereas the needle contacted to surface areas, differing in mechanical properties. The scanning pitch was established by selecting linear dimensions of a scanning area and a number of pitches 256×256. A few (usually 2 or 3) test areas were singled out on every specimen to fulfill a series of scannings with successive diminishing of the scanning area scale from 10–20 to 1–2 μm.

Micromorphology of the primary mineral surface and the surface of mineral specimens treated with acid solutions was examined on both polished sections and natural cleavages. After treatment with acid solutions the test specimens were washed with distilled water, dried in air under standard conditions, and subjected to microscopic examination.

AFM images were processed and analyzed by applying NOVA, ImageAnalysis 2.0 (NT-MDT, Russia) and SPIP 6.4.4 (Image Metrology A/S) software. Reliability of test data was verified by preliminary sampling of images exactly representing the specific morphology of the initial mineral surface.

The phase composition of the rare metal particle surface was analyzed by X-ray photoelectronic spectroscopy at Kratos Axis Ultra DLD spectrometer with monochromatic X-ray source AlK_α, energy 1486.6 eV, emission current 20 mA, voltage 10 kV, the analytical cell pressure below or equal to 10^{-8} Pa. The energy bond scale (E_b) of the spectrometer preliminarily calibrated according to position of peaks of basic levels Au $4f_{5/2}$ (E_b = 83.96 eV), Ag $3d_{5/2}$ (E_b = 368.21 eV), and Cu $2p_{3/2}$ (E_b = 932.62 eV) in spectra of the surface of elementary reference specimens (gold, silver, and

copper), calibration precision being ± 0.05 eV. The spectra were recorded with the use of a neutralizer in order to eliminate the effect of specimen charging. The resultant spectra were calibrated by bond energy of a low-energy component in spectrum C 1*s*-electron level adsorbed onto surface of hydrocarbons which bond energy was assumed equal to 284.8 eV. Inelastic losses of electron energy were subtracted by Shirley method.

XPE spectra were recorded at constant energy bandwidth of the analyzer 160 eV for overall spectra and 40 eV for spectra of internal electron levels of basic elements: Nb 3*d*, Ta 4*f*, Zr 3*d*, Fe 2*p*, Mn 2*p*, O 1*s*, and Si 2*p*. Overall spectrum was recorded at 1 eV pitch, spectra of individual lines were recorded at 0.05 eV pitch. The conventional Casa XPS software procedures were employed to process spectra of individual lines of the elements in order to obtain qualitative and quantitative information on mineral surface composition. The XPES examination of mineral surface is described in [9, 10].

The efficiency of mineral suspension treatment with anolyte and chloride solution was assessed by intensity of variations in physicochemical properties of the liquid phase and electrochemical (electrode potential φ, mV), electrical (ζ-potential, mV), electrophysical (electrostatic surface potential V, mV), and mechanical (Vickers microhardness, HV, MPa) properties of the minerals.

Electrochemical properties of the minerals, viz., drainless electrode potential were measured with potentiometric titration with concurrent monitoring of mineral potential and medium pH [6, 11]. The working electrodes were made of discrete columbite and tantalite grains of ~2 mm in size with no inclusions and defects, visual through binocular microscope. Contact line was fixed to every grain with conductive adhesive. Next the test specimens were poured with EpoThin® (Buehler) epoxy resin; after hardening the resultant blocks were finished by special techniques and equipment (Labotom-3 cut–off machine and RotoPol-35 grinding and polishing precision machine) to prepare test working specimens. The electrode surface was finally finished with MetaDi (Buehler) polycrystalline pastes under microscopic control of polished surface grade.

Mineral electrodes were placed in succession into the measuring chamber of 250 cm^3 in volume filled with muriatic solution or anolyte to measure variations in electrode potential φ versus medium pH at laboratory electrochemical analyzer of MultitestIPL–513 series. The saturated chlorosilver electrode was selected as the reference electrode.

Electrokinetic potential of mineral particles of less than 10 μm in size was measured with the dynamic (electrophoretic) light scattering at Zetasizer Nano ZS universal test system (Malvern Instruments) for nano-particles. *Z*-potential was measured in distilled water, muriatic solution and anolyte.

Electrostatic potential of natural tantalite cleavage surface was quantitatively evaluated on the basis of the Calvin probe force microscopy (CPFM) data [12, 13]. The application of two-passes Calvin's probe procedure permits to eliminate appreciably the topographic component effect on the surface distribution pattern of the electrostatic potential [12–15]. In the first pass the surface relief was recorded, the distribution of *Z*-component of the surface potential gradient on the specimen surface was measured in the second pass of the cantilever, when the needle elevated by Δz distance over the specimen and $\Delta z \sim 5$–10 nm [12, 13]. In Calvin-probe technique the special base with ground contact was used to place the specimen and the high–resolution silicone AFM cantilevers of NSG10/TiN series with TiN conductive covering on the side of the needle, resonance frequency ~260 kHz, stiffness constant 11.8 N/m, needle curvature radius 35 nm.

Microhardness of columbite, tantalite, and zircon before and after treatment with anolyte and muriatic solution was evaluated by Vickers method (HV, MPa) under GOST-2999-75 (ISO 6507–1 : 2005) at PMT-3M microhardometer, equipped with FOM-2 photoelectric ocular micrometer at 100 g loading of an indenter for 10–15 s. Microhardness in Vickers method was calculated by

$HV = (0.189P/d^2)\cdot 10^6$, where P is normal load applied to diamond tip, N; d is arithmetic average of both diagonal lengths of the indent, μm. In all the tests on measurement of microhardness of minerals the difference of indent diagonal length values for diamond tip, pressed into section surface, was not higher than 3%. The similar procedure for the mineral surface microhardness measurement is reported in [16, 17].

2. ANALYSIS AND DISCUSSION OF EXPERIMENTAL RESULTS

2.1. Analytical Electronic Microscopy

Tantalite specimen is a large-size concretion (3×2×2 cm) of short-prism-shaped crystals (Fig. 2a), in the form of a blocked quartz–microcline aggregate. Quartz–microcline contacts are well-defined with inductive surfaces of joint growth. Tantalite is macroscopically black with irregular fracturing and submetallic luster. Surface of crystals are tarnished in places, fiber-like strings of feldspar and apatite can be seen in jointing of tantalite aggregate. Indigenous quartz and microcline inclusions are traced. There are also feldspar resorption voids. Tantalite cleavage surface is visually clean while quartz and microcline, surrounding tantalite, are covered with limonite films and dendritic manganese hydroxide cakes.

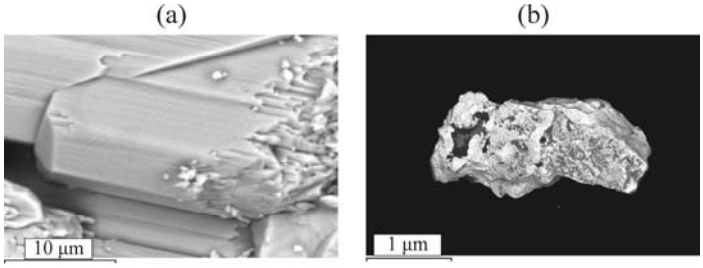

Fig. 2. (a) Flattened short-prism-shaped tantalite crystals and (b) isometric columbite grains.

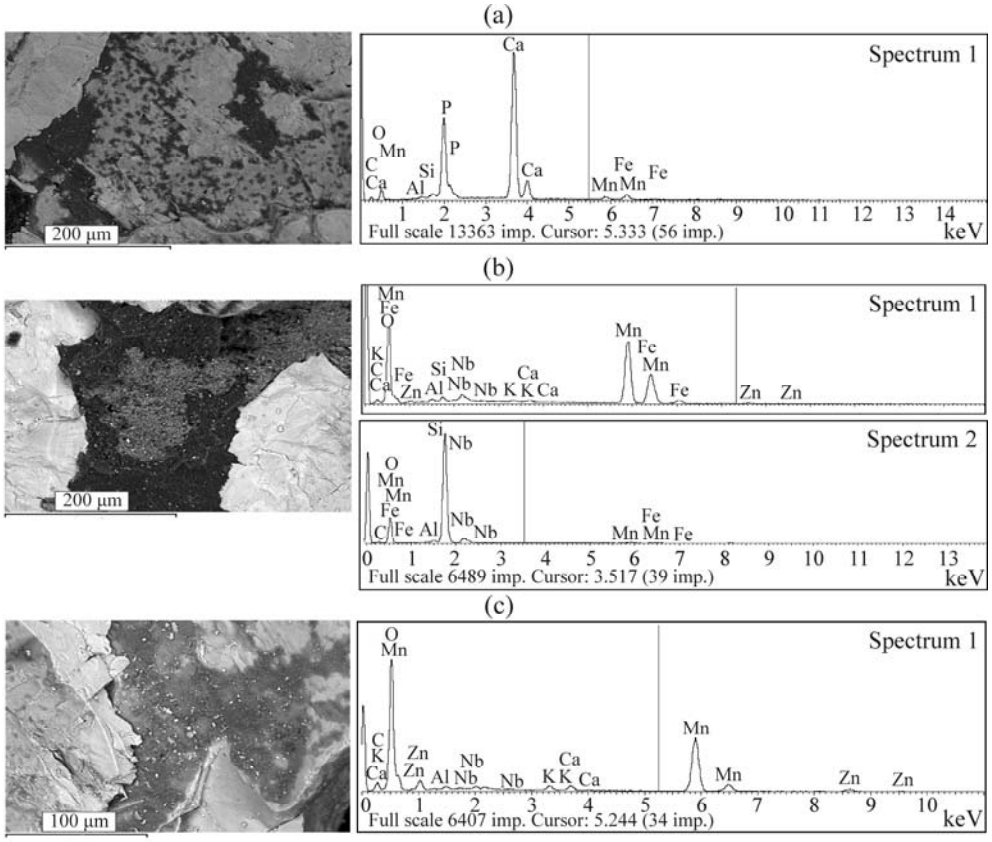

Fig. 3. (a) Disseminated apatite in columbite; (b) fractures stuffed with manganese hydroxides and quartz; (c) Mn hydroxide films; X-ray spectra of (a) apatite, (b) quartz, (b), (c) manganese hydroxides.

Columbite is macroscopically black with brownish shade, irregular or even flinty fractures, submetallic luster (Fig. 2b). Discrete mineral grains are distinguished for fragmental crystalline faceting. According to XEM data columbite contains microscopic disseminated apatite (Fig. 3a) and fractures stuffed with quartz and manganese hydroxides (Figs. 3b and 3c).

Zircon is represented with discrete bipyramidal individuals of ~300 μm in size (Fig. 4a) and fragments of larger size crystals. Facets of crystals are covered with iron and manganese hydroxides films, the latter are absent on surface of fractures (Fig. 4b). In some cases epitaxial growth of thorite ($ThSiO_4$) is detected on facets of bipyramidal zircon.

Quartz specimens of $-3+0.5$ mm in size were of two kinds: the first was opaque, yellowish, oval, the second was transparent, angular, with cutting edges, flinty fractures being fragments of larger size individuals. Color of the first–kind grains is due to iron hydroxides inclusions in both grain volume and grain surface (Fig. 5a). The second–kind grains are of higher purity, iron hydroxides responsible for color are localized in fractures of primary large grains. The distribution of these more massive and dense films on quartz surface is less regular. The first kind seems to be represented with metasomatic quartz and the second kind does with magmatic quartz.

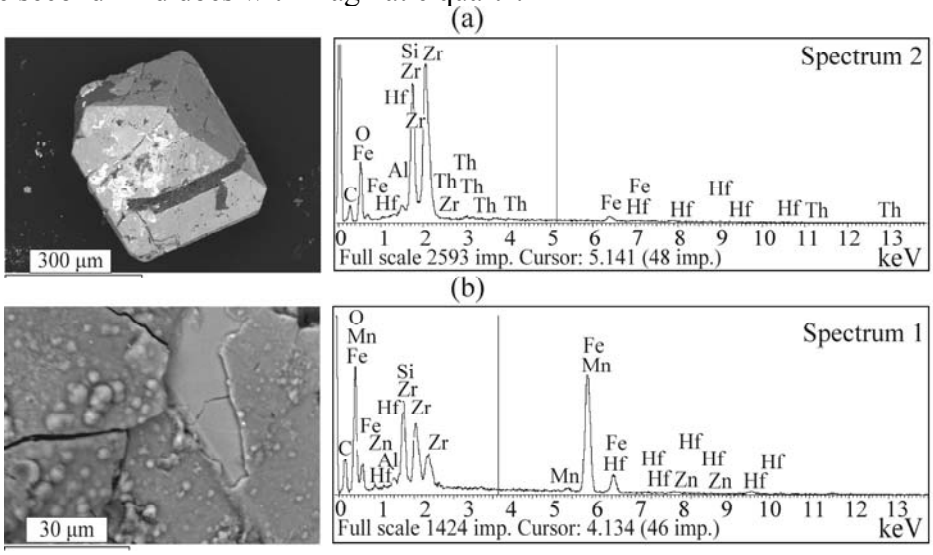

Fig. 4. Bipyramidal zircon crystal with (a) thorite growth and (b) iron–manganese film on facets; X-ray spectra of (a) thorite microinclusions and (b) surface film.

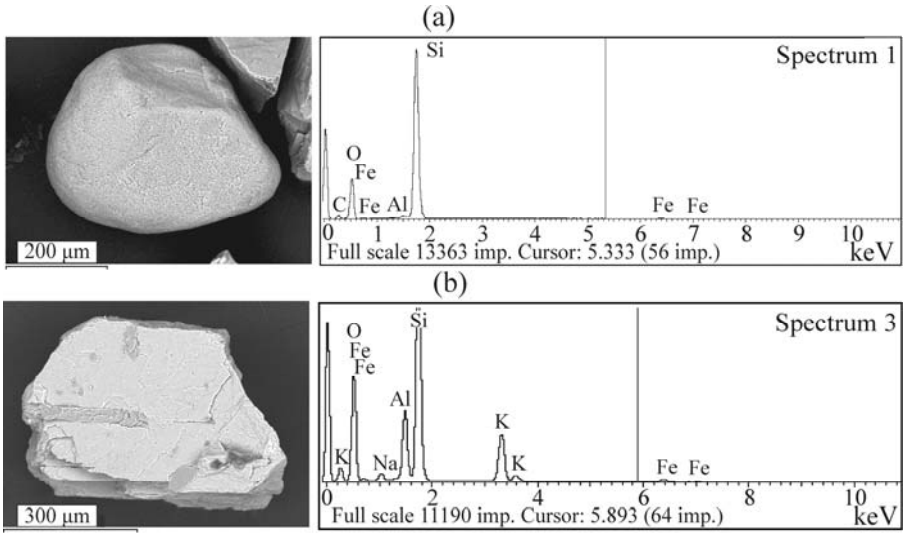

Fig. 5. (a) Quartz grains with iron hydroxide film and (b) feldspar and the related X-ray spectra.

Feldspar concentrate– 1 + 0.3 mm in size consists of macroscopical monomineral tabular cleavage flakes from lucid to translucent transparency (Fig. 5b). From colorless to yellowish–brown color of mineral particles is due to different thickness of ferritization film. As for the mineral composition (see Table 1) microcline with cryptoperthite albite ingrowths is present at ratio 78/22 mol %. The feldspar composition throughout the area is in compliance with initial magmatic mineral $(K_{0.78}Na_{0.22})(Al_{0.96}Si_{3.04})O_{8.02}$. Nevertheless spots of $K_{0.97}(Al_{0.94}Si_{3.06})O_{8.02}$, specific for pure microcline are detected within this area. Albite ingrowths are so fine that XEM technique fails to detect them.

2.2. X-Ray Photoelectronic Spectroscopy

Overall XPE spectra of tantalite, columbite, and zircon surface contain specific peaks of core level of tantalum, columbite, zircon, iron, manganese, oxygen, and silicium (Table 2). Photoelectronic spectrum of Ta 4*f* level in columbite and tantalite compositions is characterized with spin-orbital doublet Ta $4f_{3/2}$ and Ta $4f_{1/2}$, which maximum position ($E_b \sim 26.0$ and 27.9 eV) corresponds to tantalum pentoxide Ta_2O_5 [18]. Doublet Nb 3*d* (E_b = 207.0 and ~ 208.9 eV) conforms the chemical state of Nb_2O_5 [19].

Table 2. Variations in phase composition of tantalite, columbite, and zircon surface under treatment of mineral specimens with HCl solution and anolyte

Mineral	XPE peak	E_b, eV	Peak rating	Initial	HCl	Anolyte
				at.%		
Tantalite	Ta 4*f*	26.0	**Ta_2O_5**	54.9	55.9	56.8
		27.9		45.1	44.1	43.2
	Nb 3*d*	206.9	**Nb_2O_5**	58.7	58.1	60.6
		208.9		41.3	41.9	39.4
	Fe 2*p*	709.5	**Fe(II)–O**	**34.4**	**23.8**	**5.0**
		711.2	**Fe(III)–O**	**52.3**	**58.3**	**36.7**
		713.2	**Fe(III)–OH**	**13.2**	**18.0**	**58.4**
Columbite	Nb 3*d*	207.1	**Nb_2O_5**	60.5	60.8	60.2
		209.9		39.5	39.2	39.8
	Fe 2*p*	709.5	**Fe(II)–O**	**19.7**	**17.6**	**3.5**
		711.2	**Fe(III)–O**	**52.1**	**56.3**	**32.4**
		713.2	**Fe(III)–OH**	**28.2**	**25.8**	**64.2**
	Mn 2*p*	640.2	**Mn(II) MnO**	**57.0**	**65.8**	**60.5**
		641.1				
		641.9	**Mn(IV) MnO_2**	**43.0**	**34.2**	**39.5**
		642.7				
Zircon	Zr 3*d*	183.0 – 183.1	**$ZrSiO_4$**	56.7	58.9	56.6
		185.0 – 185.1		43.3	41.1	43.3
	Si 2*p*	101.7 – 102.1	**$ZrSiO_4$**	**39.3**	**35.1**	**30.2**
		103.0 – 103.2	**SiO_2, Si–OH**	**60.8**	**64.8**	**69.8**
	O 1*s*	531.1 – 531.3	**$ZrSiO_4$**	**49.9**	**32.6**	**45.6**
		532.0 – 532.3	**SiO_3^{2-}, SiO_2^0**	**50.1**	**67.4**	**54.4**

In Mn 2*p* manganese spectrum the following maximums: $E_b \sim 640.2$, 641.1, 641.9, 642.6, 643.6 eV are singled out. First two maximums refer to state of MnO, namely, Mn(II), the rest do to Mn (IV) [20]. Spectrum Fe $2p_{3/2}$ is approximated by using parameters [21] and three components are pointed out: band 709.5 eV refers to Fe^{2+}, bonded with oxygen; bands 711.2 eV and 713.3 eV are for Fe^{3+} in oxide and hydroxide states, respectively.

In Zr 3*d* XPE spectrum two components are identified with energy bonds equal to $E_b \sim 183.0$ and 185.1 eV, specific for zircon atoms in structure $ZrSiO_4$. In Si 2*p*-electrons spectrum two chemical states of silicium are specified [22, 23]: silicium in zircon composition $E_b = 101.7$–102.1 eV and Si atoms involved into chemical states SiO_2 and Si–OH ($E_b = 103.0$–103.2 eV). The band of O 1*s*-oxygen atom level in the study zircon specimens can be represented as the superposition of two components corresponding to three-coordinated oxygen in structure $ZrSiO_4$ with $E_b = 531.1$–531.3 eV and oxygen atoms in the composition of defect groups, such as SiO_3^{2-}, SiO_2^0 with $E_b = 532.0$–532.3 eV [22] (Table 2).

The analysis of XPES data made it possible to conclude that treatment of rare metal minerals with both HCl solution and anolyte did not appreciably influence the chemical state of tantalum, niobium, and zirconium atoms in the mineral composition (Table 2). The basic aftereffect of physicochemical action of acid solutions on valent state of atoms on mineral surface manifests as oxidation of iron atoms with transition of Fe(II) to Fe(III) for columbite and tantalite (Fig. 6) and destruction of zircon surface with formation of oxygen–vacancy defects (Fig. 7).

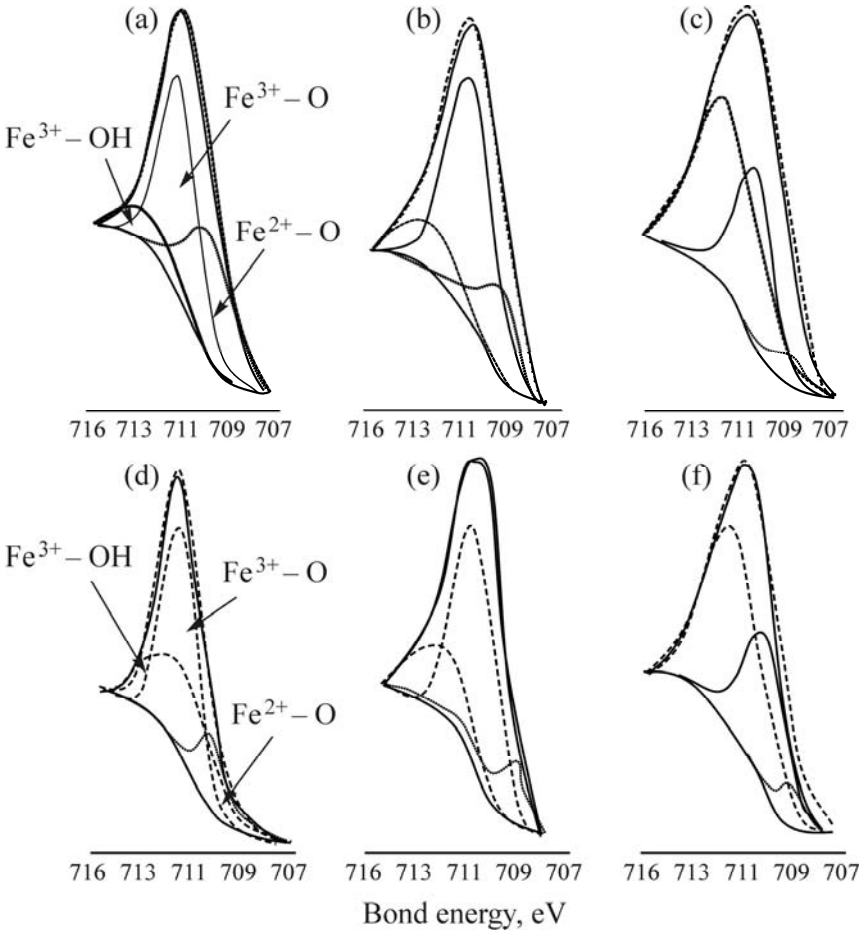

Fig. 6. XPE spectra of Fe 2*p*-iron level on (a)–(c) tantalite particle surface and (d)–(f) columbite (a), (d) before and (b), (e) after treatment with (b) HCl solution and (c), (f) anolyte.

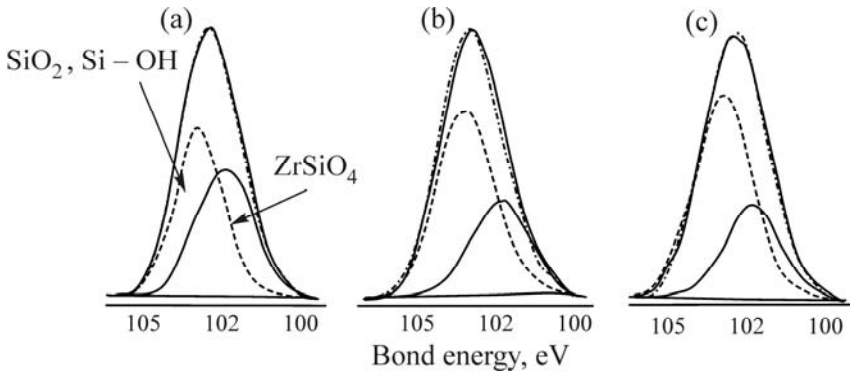

Fig. 7. XPE spectra of Si 2*p*-silicium level on zircon particle surface (a) before and after treatment with (b) HCl solution and (c) anolyte.

Treatment of tantalite with anolyte resulted in growth of the total Fe(III) content by 9.5 at.% at essential domination of hydroxide phase Fe(III)–OH (Table 2). Given that the mineral contacted to HCl solution, the total increment in Fe(III)–O and Fe (III)–OH reached 10.7 at.%.

The use of HCl solution for columbite did not substantially increase surface Fe(III) concentration, nevertheless treatment of the mineral with anolyte induced intensive oxidation of iron atoms with transition of Fe(II) to Fe(III) (Table 2). Thereto, actually all the surface iron 96.5 at.% was ferric, hydroxyl Fe(III)–OH amounted to 64.2 at.%. Along with alteration of chemical state of surface iron atoms in columbite composition the treatment of the mineral with either anolyte or HCl solution boosted surface Mn(II) concentration proportionally to decrease in Mn (IV) concentration (Table 2) presumably due to reduction of Mn(IV) atoms to Mn(II).

XPE spectra for Si 2*p* and O1 *s* zircon indicate essential variations in structural–chemical state of surface mineral atoms under treatment with acid solutions. According to the analysis of Si 2*p*-silicium atom level band (Fig. 7) the leaching effect of solutions caused partial transition from 4 to 9 at.% of Si atoms from $ZrSiO_4$ to the chemical state close to SiO_2^0 (Table 2). When the mineral is treated with HCl solution, the spectrum of O 1*s* core states shows appreciable growth of the component with $E_{b.} = 532.3$ eV, corresponding to oxygen atoms in defected surface clusters, having SiO_3^{2-} and SiO_2^0 structure [22] (Table 2).

2.3. Physicochemical Properties of the Liquid Phase of Mineral Suspensions

According to experimental evidence on variations in composition and physicochemical properties of the liquid phase of mineral suspensions (Table 3) the use of anolyte provokes 1.2–1.5 times increase in iron and silicium ion concentration in the solution as compared to the treatment with HCl solution.

In the treatment of columbite with anolyte Fe(III) concentration in the liquid phase of the mineral suspension ($6.3 \cdot 10^{-8}$ mg·cm^{-2}) exceeded 8.6 times respective concentration ($0.73 \cdot 10^{-8}$ mg·cm^{-2}) in HCl solution, perhaps due to the active oxygen adsorption by columbite surface as redox potential of anolyte solution is displaced from + 845 to + 300 mV.

The active oxidation of iron on mineral surface is confirmed by increased concentration of total iron content in the liquid phase. When rusty quartz was treated with anolyte for 1 hour, an amount of iron ($C'(\text{Fe})$, Table 3), dissolved from mineral surface was 1.5 times higher than $C'(\text{Fe})$ value, obtained in treatment of quartz with HCl solution: $2.1 \cdot 10^{-6}$ and $1.4 \cdot 10^{-6}$ mg·cm^{-2}, respectively.

Thus, the treatment of mineral suspensions with anolyte provided not only more effective resorption of iron- and silicate-containing films from mineral surface as compared to the effect of HCl solution, conventionally practiced in well–established processes [1, 2], but also the active oxidation of ferrous iron into ferric iron in the crystalline lattice of columbite and tantalite. The spectroscopic and physicochemical examination data are verified with measurements of drainless electrode and electrokinetic potentials of minerals in aqueous and acid media.

Table 3. Variations in physical–chemical properties of the liquid phase of mineral suspensions under anolyte and HCl solution treatment

Treatment	pH_s*	pH_f*	Eh_s	Eh_f	Concentration					
					Fe(III)	Fe(II)	Mn	O_2	SiO_2	C'(Fe)
					(mg×cm^{-2})×10^{-8}				(mg×cm^{-2})×10^{-6}	
Columbite										
In anolyte	3.4	6.5	+845	+300	6.3	17.7	17.6	58	—	—
In HCl solution	3.4	6.4	+525	+390	0.7	17.9	18.3	13	—	—
Zircon										
In anolyte	3.1	6.0	+700	+280	4.9	1.8	—	262	12	—
In HCl solution	3.1	5.5	+550	+320	4.4	1.5	—	35	5.8	—
Quartz										
In anolyte	3.1	6.2	+690	+300	0.4	0.29	—	36	2.5	2.1
In HCl solution	3.1	5.9	+550	+310	0.1	0.1	—	7.4	1.4	1.4
Feldspar										
In anolyte	3.1	6.5	+700	+260	10.9	2.2	—	121	—	—
In HCl solution	3.1	6.5	+550	+320	2.9	0.4	—	0.4	—	—

*Indices "s" and "f" are for start and finish of the treatment·

2.4. Electrochemical and Electric Properties of Minerals

The investigation into electrochemical properties of columbite and tantalite surface (Fig. 8) justified that the treatment of the mineral with anolyte shifted the drainless electrode potential by 200–250 mV for columbite and by 20–80 mV for tantalite to the positive value domain as compared to the use of HCl solution (Table 4). The experimental results comply with XPEM data (Table 2), which confirmed that when treating the mineral with anolyte, iron atoms were intensively oxidized with increasing Fe(III)/Fe(II) ratio on mineral surface (in the greater degree for columbite) thanks to manifestation of strong oxidizing properties of anolyte under conditions of higher concentration of electrolytic oxygen in the solution (Table 3) [4].

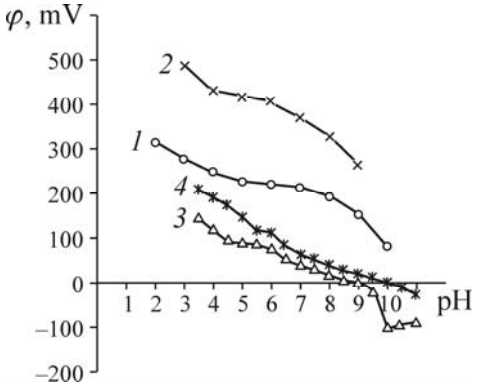

Fig. 8. Variations in electrode potential: *1*, *2*—columbite; *3*, *4*—tantalite in the solution *1*, *3*—HCl; *2*, *4*—anolyte vs. medium pH.

Table 4. Variations in electrochemical, electrical, and mechanical properties of rare metal minerals in treatment with HCl solution and anolyte

Mineral	φ, mV(pH 3.5)		ζ-potential, mV		V, mV		HV, MPa		
	Treatment (i/s—initial state)								
	HCl solution	Anolyte	HCl solution	Anolyte	i/s	Anolyte	i/s	HCl solution	Anolyte
Columbite	270	460	9.4	2.4	—	—	953	796.4	726
Tantalite	140	190	1.6	3.1	−16.9	−39.4	984	893	757.5
Zircon	—	—	10.2	−8.6	—	—	1280.5	1161.5	1079

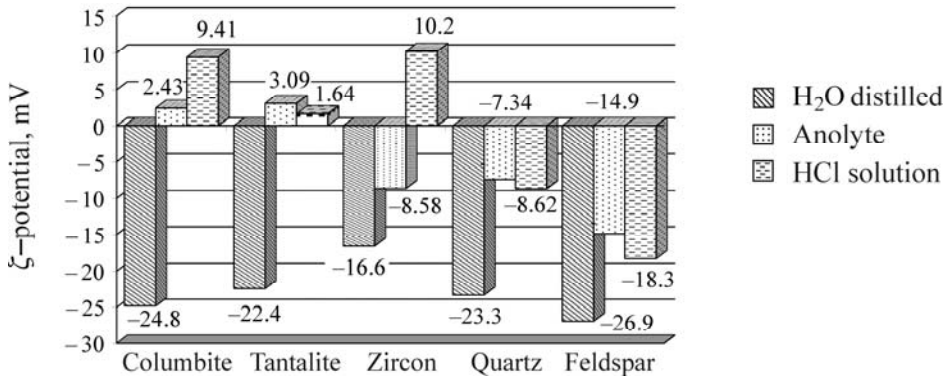

Fig. 9. Variations in ζ-potential of minerals under treatment with HCl solution and anolyte.

The surface layers of columbite and tantalite are characterized with presence of positively charged cations Fe(II) and Mn(II), as well as hydrated iron oxides in the form of self-contained surface phases. Electrical potential of mineral particle surface, suspended in the liquid phase, is evaluated by resorption of ions from mineral crystal surface and their transition to the liquid phase with generation of a crystal surface charge in the course of resorption [24]. Potential-refining ions are cations of iron and manganese nearby columbite and tantalite surface; counter-ions are hydroxyl groups (hydroxide anions) of the liquid phase, this state of things determines the negative sign of ζ-potential of columbite and tantalite in the neutral medium pH 7 (Fig. 9).

Addition of HCl solution to the test system initiated selective adsorption of chloride anions on columbite (tantalite) surface. The surplus negative charge was generated on mineral surface along with surplus positive charge (hydrogen ions) in the nearby solution layer, viz., the double electric layer (DEL) originated on the interphase surface. The diffusion part of DEL is positive, so ζ-potential was displaced to the domain of positive values (Fig. 9, Table 4).

In anolyte treatment of the mineral the oxygen was actively adsorbed by mineral surface, thus promoting oxidation of Fe(II) to Fe(III) according to the pattern $\text{Fe(II)} + \rightarrow \text{Fe(III)} + e^-$. The dissolution of surface hydroxide films proceeded concurrently along with leaching of Fe(III) and Mn(II) cations from crystalline lattice of the surface columbite layer. The above processes disturbed electrical neutrality of the surface, generated the surplus negative charge (anions of the liquid phase) on the mineral surface and the surplus positive charge (hydrogen ions) in a nearby solution layer. Thus DEL was also generated on interphase surface, its diffuse component was positive and the electrokinetic potential had positive sign (Fig. 9, Table 4).

Variations in ζ-otential of zircon and rock minerals in the treatment with anolyte and HCl solution (Fig. 9) were in good compliance with the data of [24–26], according to which the electrokinetic potential of minerals tends to move to the domain of negative values with increasing pH of the liquid phase. In leaching of mineral suspensions iron hydroxides were removed from surface of zircon, quartz, and feldspar with formation of spots of oxygen-vacant defects with SiO_3^{2-}, SiO_2^0 structure in the surface layer of the minerals (zircon and quartz) [22]. This apparently promoted generation of the surplus negative charge on mineral surface, DEL formation with the positive diffuse layer, and ζ–potential displaced to the domain of positive values (Fig. 9).

2.4. Atomic Force (Electroforce) Microscopy and Microhardness Testing

According to atomic force microscopic data in the initial state (no treatment with anolyte or HCl solution) the surface of tantalite section was characterized as a grained structure with fine densely adjoined elongated species of 60–100 nm in size (Fig. 10a); the natural cleavage surface of the minerals contained terraces, micro- and nano-size scratches made by polishing materials. The correlation was pointed out in images of the relief, phase contrast and electrostatic potential of tantalite surface in Fig. 10, moreover, the maximum values of phase contrast and potential (in lighter colors) corresponded to dents on specimen surface and to intergrain boundaries.

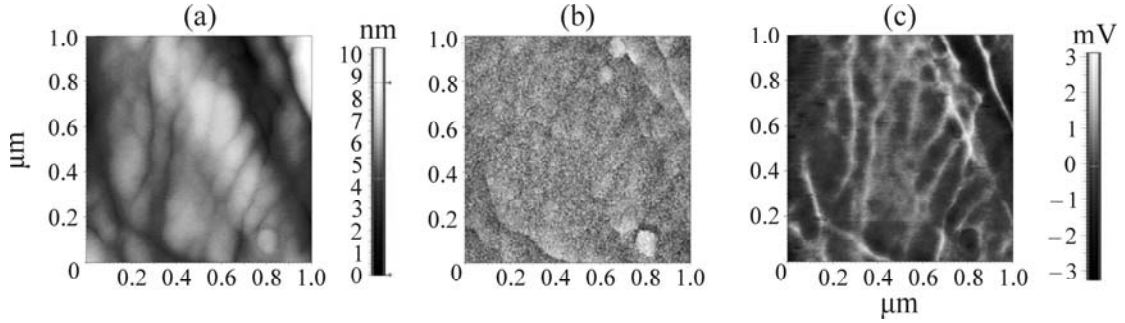

Fig. 10. AFM images of (a) the relief, (b) phase contrast, and (c) electrostatic potential of the initial tantalite specimen surface. Scan size is 1×1 μm.

When treating the tantalite section with HCl solution, the effect of selective mineral surface etching was observed in spots of defect localization, viz., scratches and microfractures (Fig. 11b) with resultant reduction in microhardness of the mineral from 984 to 893 MPa (Table 4). The quantitative analysis of AFM images revealed roughening of the surface relief as a whole, increase in amplitude (height) of roughness, namely, averaged quadratic S_q and averaged arithmetic S_a roughness from 2.4 and 1.9 to 2.7 and 2.2 nm, respectively. In lateral direction microdefect boundaries (microfracture opening) were expanded from 23–30 nm to 46–50 nm.

After tantalite was treated with anolyte, two dissimilarities were established for the altered mineral surfaces with different morphological features depending on a type of test specimens: polished section and natural cleavage (Fig. 11). The surface of polished section was characterized with uniformly located defects–microcavities (dents) of semispheric shape of ~60 nm in diameter (Fig. 11c), commensurable with size of particles made of densely packed fragments of mineral surface in the after-polished state. The electrochemical treatment of tantalite might provoke activation of leaching and partial dissolution of iron-containing films in extruding spots and intergrain contacts and induced the formation of surface relief with morphological pitting (spot) corrosion features. The established variations in roughness parameters S_q and S_a from 1.5 and 1.2 nm to 1.1 and 0.8 nm, respectively, indicated the negligible relief smoothing of the initially polished mineral surface.

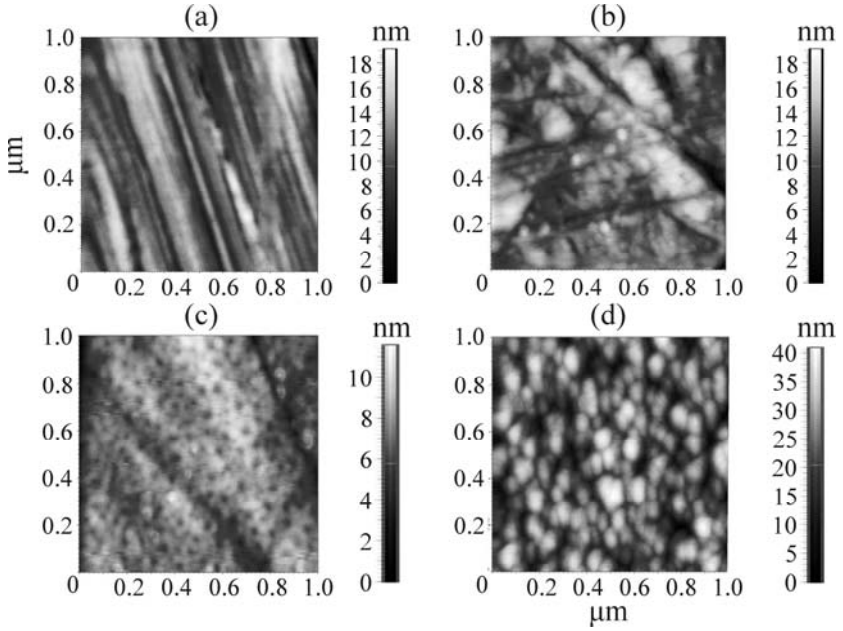

Fig. 11. AFM images of (a), (b), (c) the section surface relief and (d) cleavage of tantalite (a) before and (b) after treatment with HCl solution and (c), (d) anolyte. Scan size is 1×1 μm.

Anolyte treatment contributed to formation of particles of finely dispersed phase on natural tantalite cleavages (Fig. 11d). As compared to the initial relief, AFM scans 1×1 μm in size demonstrated high isolation of particles, sharp intergrain boundaries and increase in S_q and S_a from 4.4 and 3.4 nm up to 7.3 and 5.8 nm, respectively, as well as average height of object images Z_{av} from 4.4 up to 6.6 nm at practically unchanged lateral dimensions of the objects.

According to the data of scanning Kelvin-probe force microscopy the values of electrostatic tantalite-surface potential vs. probe potential are negative for all the study surface areas with the most typical morphology (Table 4) [15]. As the mineral was treated with anolyte, the potential values displaced by 18–22 mV (depending on scanning scale) to the domain of negative value, perhaps due to partial removal of Fe(II) cations from tantalite surface and their transition to the leaching solution along with generation of surplus negative charge on the surface of altered crystal.

The structural–chemical transformations of tantalite surface (Mohs' hardness is 5.5–6) under anolyte influence caused reduction in mineral hardness from 984 to 757.5 MPa (Table 4). The relative variation in tantalite crystal microhardness is $\Delta HV = (HV_{0i} - HV_i)/HV_{0i}$,%, where HV_{0i}—microhardness of specimens in the initial state; HV_i—microhardness of i-th specimen after treatment with HCl solution or anolyte was 9.2 and 23%, respectively. Columbite (Mohs' hardness is 6–6.5) reduced microhardness of crystals from 953 to 796.4 MPa when treated by HCl solution and down to 726 MPa after treatment with anolyte (Table 4). The relative variations in microhardness of the mineral were 16.4 and 23.8% after treatment with HCl solution and anolyte, respectively.

The leaching solutions caused destruction of zircon surface with formation of oxygen containing spot defect complexes of oxygen–vacancy (O–V) type and /or $Si_xV_yO_z$ type [22, 27] and efficient weakening of the surface of high-hardness mineral (Mohs' hardness is 7–8) as a consequence. The acid and indirect electrochemical treatment of the specimens lowered microhardness of the mineral from 1280.5 MPa (initial state) down to 1161.5 MPa (after treatment with HCl solution) 1079 MPa (after anolyte treatment) (Table 4); ΔHV of zircon was 9.3 and 15.7% for treatment with HCl solution and anolyte, respectively.

In closing, the treatment of mineral suspensions with anolyte ensures more efficient dissolution of iron- and silicate-containing films from mineral surface and active oxidation of bivalent iron to three-valence metal in crystalline lattice of columbite and tantalite, and formation of oxygen–vacancy defects on zircon surface. The spectroscopic and microstructural examination data were verified with latest experimental data on targeted variation in physical–chemical, electrical, and mechanical properties of tantalite, columbite, zircon, and feldspar by leaching minerals with acid solutions and preferable use of anolyte alternatively to HCl solution.

CONCLUSIONS

The present investigation promoted the establishment of the mechanism for structural–chemical surface transformations of tantalite, columbite, and zircon in leaching with acid solutions, including activation of dissolution of iron- and silicate-containing films from the mineral surface, and intensive oxidation of iron atoms in the surface layer of tantalite and columbite with transition of Fe(II) to Fe(III) and destruction of zircon surface with formation of oxygen–vacancy defects of SiO_3^{2-}–, SiO_2^0-types under anolyte treatment.

It was experimentally substantiated and verified the feasibility and higher efficiency of acid water-electrolysis product (anolyte) for targeted alteration of chemical and phase composition of the surface,

physicochemical, electrochemical, electrical, and mechanical properties of tantalite, columbite, zircon, and feldspar as compared to HCl solution, practiced in conventional finishing preparation of rough tantalum–niobium gravity concentrates for flotation.

ACKNOWLEDGMENTS

The work was supported by the Russian Science Foundation, project no. 16-17-10061.

REFERENCES

1. Solodov, N.A., Usova, T.Yu., Osokin, E.D., et al., *Netraditsionnye tipy redkometall'nogo mineral'nogo syr'ya* (Alternative Raw Rare Metal Mineral Materials), Moscow: Nedra, 1990.
2. Maslov, A.A., Ostvald, R.V., Shagalov, V.V., et al., *Khimicheskaya tekhnologiya niobiya i tantala* (Chemical Niobium and Tantalum Technology), Tomsk: TPU, 2010.
3. Bogdanov, O.S., Gol'man, A.M., Kakovsky, I.A., et al., *Fiziko-khimicheskie osnovy teorii flotatsii* (Physicochemical Fundamentals of Flotation Theory), Moscow: Nauka, 1983.
4. Chanturia, V.A., Konev, S.A., Ishchenko, V.V., et al., Investigation into Processes on Tantalite–Columbite Surface under Polarization, *Kompleks. Isp. Min. Syr'ya*, 1985, no. 12, pp. 16–20.
5. Betekhtin, A.G., *Kurs mineralogii* (Mineralogy: Textbook), Moscow: Knizh. Dom Univer., 2010.
6. Chanturia, V.A. and Shafeev, R.Sh., *Khimiya poverkhnostnykh yavlenii pri flotatsii* (Surface Chemistry in Flotation), Moscow: Nedra, 1977.
7. Plaksin, I.N., Shafeev, R.Sh., and Chanturia, V.A., Energy Structure–Flotation Properties Interaction in Mineral Crystals, in Plaksin I.N., *Izbrannye trudy. Obogashchenie poleznykh iskopaemykh* (Selectas. Mineral Processing), Moscow: Nauka, 1970, pp. 136–147.
8. Plaksin, I.N. and Shrader, E.A., *O vzaimodeistvii flotatsionnykh reagentov s nekotorymi nesul'fidnymi mineralami redkikh metallov* (Interaction of Flotation Agents with Non-Sulfide Rare Metal Minerals), Moscow: Nauka, 1967.
9. Briggs, D. and Seah M.P., *Practical Surface Analysis by Auger and X-Ray Photoelectron Spectroscopy*, Chichester, New York: John Wiley and Sons Ltd, 1983.
10. Chanturia, V.A., Bunin, I.Zh., Ryazantseva, M.V., Khabarova, I.A., X-Ray Photoelectron Spectroscopy-Based Analysis of Change in the Composition and Chemical State of Atoms of Chalcopyrite and Sphalerite Surface before and after the Nanosecond Electromagnetic Pulse Treatment, *J. Min. Sci*., 2013, vol. 49, no. 3, pp. 489–498.
11. Chanturia, V.A. and Vigdergauz,V.E., *Elektrokhimiya sul'fidov. Teoriya i praktika flotatsii* (Sulfide Electrochemistry. Theory and Practice of Flotation), Moscow: Ruda Metally, 2008.
12. Mironov, V.L., *Osnovy skaniruyushchei zondovoi mikroskopii* (Scanning Probe Microscopy Fundamentals), Moscow: Tekhnosfera, 2005.
13. Melitz, W., Shena, J., Kummel, A.C., and Lee, S., Kelvin Probe Force Microscopy and its Application, *Surface Science Reports*, 2011, vol. 66, no. 1, pp. 1–27.
14. Nazarchuk, Yu.N., Novikov, V.A., and Torkhov, N.A., Investigation into Influence of Local n-GaAs Surface Metallization Size on Surface Potential Distribution Pattern Obtained by Atomic Force Microscopy, *Izv. Vuzov. Physics*, 2011, no. 3, pp. 32–35.
15. Rudinsky, M.E., Gutkin, A.A., and Brunkov, P.N., Electrostatic Potential of Epitaxial InN Layer Surface and its Variation under Anode Oxidation, *Poverkh. Rentg. Sinkhrotr. Neitr. Issled*., 2012, no. 5, pp. 48–52.

16. Bunin, I.Zh., Chanturia, V.A., Anashkina, N.E., and Ryazantseva, M.V., Experimental Validation of Mechanism for Pulsed Energy Effect on Structure, Chemical Properties and Microhardness of Rock-Forming Minerals of Kimberlites, *J. Min. Sci*., 2015, vol. 51, no. 4, pp. 799–810.
17. Viktorov, S.D., Golovin, Yu.I., Kochanov, A.N., Tyurin, A.I., et al., Micro- and Nano-Indentation Approach to Strength and Deformation Characteristics of Minerals, *J. Min. Sci*., 2014, vol. 50, no. 4, pp. 652–659.
18. Ispas, A., Adolphi, B., Bund, A., and Endres, F., On the Electrodeposition of Tantalum from Three Different Ionic Liquids with the Bis (Trifluoromethyl Sulfonyl) Amide Anion, *Physical Chemistry, Chemical Physics*, 2010, no. 12, pp. 1793–1803.
19. Ozer, N., Chen Din-Guo, Lambert, C.M., Preparation and Properties of Spin-coated Nb_2O_5 Film by the Sol-gel Process for Electrochromic Application, *Thin Solid Films*, 1996, vol. 277, nos. 1–2, pp. 162–168.
20. Biesinger, M.C., Payne, B.P., Grosvenor, A.P., et al., Resolving Surface Chemical States in XPS Analysis of First Row Transition Metals, Oxides and Hydroxides: Cr, Mn, Fe, Co, and Ni, *Applied Surface Science*, 2011, vol. 257, no. 7, pp. 2717–2730.
21. Jung, R.-H., Tsuchiya, H., and Fujimoto, Sh., XPS Characterization of Passive Films Formed on Type 304 Stainless Steel in Humid Atmosphere, *Corrosion Science*, 2012, vol. 58, pp. 62–68.
22. Shchapova, Yu.V., Votyakov, S.L., Kuznetsov, M.V., and Ivanovsky, A.L., Effect of Radiation Defects on Electronic Zirconium Structure Based on X-Ray Photoelectronic Spectroscopy Data, *Zh. Strukt. Khimii*, 2010, vol. 51, no. 4, pp. 687–692.
23. Marshall, G.M., Patarachao, B., Moran, K., and Mercier P.H.J., Zircon Mineral Solids Concentrated from Athabasca Oil Sands Froth Treatment Tailings: Surface Chemistry and Flotation Properties, *Minerals Engineering*, 2014, vol. 65, pp. 79–87.
24. Chanturia, V.A., Role of Electrochemical and Semiconductive Properties of Minerals in Flotation, in Laskorina, B.N. and Plaksina, L.D., *Fiziko-khimicheskie osnovy teorii flotatsii* (Physicochemical Fundamentals of Flotation Theory), Moscow: Nauka, 1983, pp. 70–89.
25. Suáreza, G., Acevedoa, S., Rendtorffa, N. M., et al., Colloidal Processing, Sintering and Mechanical Properties of Zircon ($ZrSiO_4$), *Ceramics Int*., 2015, vol. 41, no. 1, Part B, pp. 1015–1021.
26. Ibrahim, I., Hussin, H., Azizil, K.A.M., and Alimon, M.M., A Study on the Interaction of Feldspar and Quartz with Mixed Anionic/Cationic Collector, *J. Fund. Sci*., 2011, vol. 7, no. 2, pp. 101–107.
27. Makara, V.A., Vasil'ev, M.A., Steblenko, L.P., et al., Variations in Impurity Composition and Microhardness of Silicium Crystal Subsurface Layers under Magnetic Field Effect, *Fiz. Tekhn. Poluprov.*, 2008, vol. 42, issue 9, pp. 1061–1064.